RESEARCH ARTICLE

Performance of a novel bent-up bars system not interacting with concrete

Aydin SHISHEGARAN[a], Mohammad Reza GHASEMI[b*], Hesam VARAEE[c]

[a] School of Civil Engineering, Iran University of Science and Technology, Tehran 13114-16846, Iran

[b] Structural Engineering, Department of Civil Engineering, University of Sistan and Baluchestan, Zahedan 98167-45845, Iran

[c] Structural Engineering, Ale Taha Institute of Higher Education, Tehran 14888-36164, Iran

[*] Corresponding author. E-mail: mrghasemi@eng.usb.ac.ir

ABSTRACT Increasing the bending and shear capacities of reinforced concrete members is an interesting issue in structural engineering. In recent years, many studies have been carried out to improve capacities of reinforced concrete members such as using post and pre-tensioning, Fiber Reinforced Polymer and other techniques. This paper proposes a novel and significant technique to increase the flexural capacity of simply supported reinforced concrete beams. The proposed method uses a new reinforcement bar system having bent-up bars, covered with rubber tubes. This technique will avoid interaction of bent-up bars with concrete. They are located in the zone where compressive and tensile forces act against one another. The compressive force in the upper point of the bent-up bars is exerted to the end point of these bars located under neutral axis. Moreover, the tensile stress is decreased in reinforcements located under the neutral axis. This will cause the Reinforced Concrete (RC) beam to endure extra loading before reaching yield stress. These factors may well be considered as reasons to increase bending capacity in the new system. The laboratory work together with finite element method analysis were carried out in this investigation. Furthermore, bending capacity, ductility, strength, and cracking zone were assessed for the new proposed system and compared with the conventional model. Both the FEM simulation and the experimental test results revealed that the proposed system has significant impact in increasing the load bearing capacity and the stiffness of the RC beams. In the present study, an equation is formulated to calculate bending capacity of a new reinforcement bar system beam.

KEYWORDS bending capacity, rubber tube, stress transfer, bent-up bars, ductility, cracking

1 Introduction

Increasing the bending capacity, ductility, and strength of the Reinforced Concrete (RC) beams have become promising concerns for structural engineers. In recent years, many experimental and theoretical studies were carried out to increase the capacities and improve the performance of RC beams. Most of such studies use shotcrete jacking, epoxy bonding the steel plates, post and pre-tensioning, Fiber Reinforced Polymers (FRPs), and other new materials or systems [1–8]. Some of these techniques are strengthened by adding an additional RC layer. Use of jackets may well be one of the most commonly and old techniques for retrofitting deficient RC members [9–11]. In recent years, this method has been popularly used because of its advantages and easy assembling system. Another words, to use externally bonded FRPs is much easier [12–15]. For instance, Figeys et al. [1] used the finite element method (FEM) and studied a case in the laboratory where a post-tensioned FRP member was stuck under a concrete beam. They compared two similar beams, one simple and one reinforced having a tensioned FRP plate. They concluded that the latter increased the beam bending capacity by nearly 40%. An easy implementation, compared with pre-tensioned cables, high capability of being initiated after the beam has been constructed and also easier maintenance are the merits of such a system [1]. Chaallal et al. [12] investigated Fiber Reinforced Bars (FRBs) and showed that they reduced cracks and increased the bending strength. Ross et al. [14]

showed that the FRP-reinforced beams gained nearly 30%–70% more bending strength; however, they lost about 40% of their ductility. Further, Smith and Teng [13] showed that concrete reinforced beams tolerate more bending and can be crushed due to steel failure or composite plate rupture; moreover, the concrete may be destroyed in the compression zone due to bending and shear cracks or the FRP plate separation from the concrete. Lee et al. [16] presented a paper entitled "Flexural strengthening of RC beams with pre-stressed Near Surface Mounted (NSM) CFRP systems" wherein eight RC beams were tested under four-point loading tests. An un-strengthened control beam was used for reference. Four beams were strengthened by pre-tension NSM CFRP bars. The test results showed that strengthening by a pre-stressed NSM beam enhanced the flexural behavior of the beam compared to that of the control beam. The post-tension NSM systems provided the best enhancement to the beam performance for the concrete cracking, steel yielding, and the ultimate loading. The reinforcement length and pre-stressing force were used as parameters to analyze the effects of the strengthening performance in the proposed numerical model. Seraj et al. [17] used heavy Pre-Stressed Concrete (PSC) and Compressive Force Path (CFP) to compare two pre-stressed sections (one without and one with two compressive forces at the beam two ends); as a result, they showed that the PSC-designed members were safer. In fact, it is noteworthy (at this level of the PSC behavior) that an excessive pre-stressing increases the shear capacity which, in turn, it increases the beam load bearing capacity. In addition, the experiments showed that under similar loading, the CFP-designed beam needs nearly 30% less reinforcement than the PSC. Recently, several investigations have involved the use of spiral reinforcements as to increase the shear capacity of beams [18–20]. Hence, a new longitudinal steel reinforcements model for beams can be an interesting topic of exploration in structural engineering as well as being the purpose of the present study.

Although most of the aforementioned methods can improve the performance or increase the capacity of RC members, they may have several issues. Difficulty of assembling, expensive implementation, durability, and resistance against fire effects are the drawbacks of these methods. Thus, introducing new methods that can be used at lower cost and ease the process of implementation with even higher capacity may always be considered a promising challenge. In this regard, Ghasemi and Shishegaran [21] used a new reinforcement bar system (NRBS) for enforcing the interconnection between compressive and tensile stresses in reinforcement bars, while there was a detached longitudinal bar in the tensile zone. The investigation was carried out by laboratory test. The bent-up bars technique was used for increasing shear capacity. However, they were placed in rubber tubes in order not to interact with concrete. It was primarily implemented by Ghasemi and Shishegaran [21] to increase bending capacity. In this research, the NRBS have two bent-up reinforcement bars placed in rubber tube avoiding interaction of bars with concrete and due to some enhancement to the system, the bending capacity was increased. In addition, verification of the FEM model was carried out for its consistency with the new accomplished laboratory test. Hence, it is necessary that the proposed NRBS beams with longer length and different bent-up reinforcement bars are built and assessed for laboratory test and also by the FEM model. In this study, the location of cracks in the FEM models are compared with the location of cracks in laboratory models for each state (beginning crack, the state of yield stress, and the state of ultimate limit). The location of crack, crack patterns, and expansion of cracks in the FEM and laboratory results are the same; therefore, the results of cracks in laboratory confirm those of the FEM.

Next, to increase the flexural capacity of simply supported RC beams, a novel technique is introduced. The proposed method uses a NRBS having bent-up bars that covered with sealed rubber tubes. The bent-up bars has no interaction with the concrete and are located in the zone which compressive and tension forces act against each other. The compressive force in upper point of the bent-up bars is exerted to the end point of these bars located under the neutral axis. Moreover, the tension stress is decreased in reinforcements under the neutral axis; therefore, they can reach yield stress having extra loading. In addition, in this study, a formula was introduced to generally enable calculating the bending capacity of RC beams, reinforced by the NRBS.

The remaining parts of this paper are organized as follows. In Section 2, the proposed system is introduced and briefly discussed. Section 3 describes the research methodology. Sections 4 and 5 introduce the FEM and experimental modeling of the proposed system, respectively, and in Section 6, the results will be compared and discussed. Finally, in Section 7, the formulation of the bending capacity of the proposed NBRS is presented.

2 Proposed system

Figure 1 shows a common simply supported beam having ordinary reinforcement bars system. As shown, the compressive and tensile stresses are created under live and dead loads above and below the neutral axis of the beam section, respectively.

By setting the load-created forces above and below the neutral axis acting against each other, the beam bending capacity can be increased; as a result, it reduces its compressive and tensile stresses, while the two forces balance each other. In the proposed system, as shown in Fig. 2, the upper reinforcement bar, one third away from both ends of the beam length is bent 45°; subsequently, it is
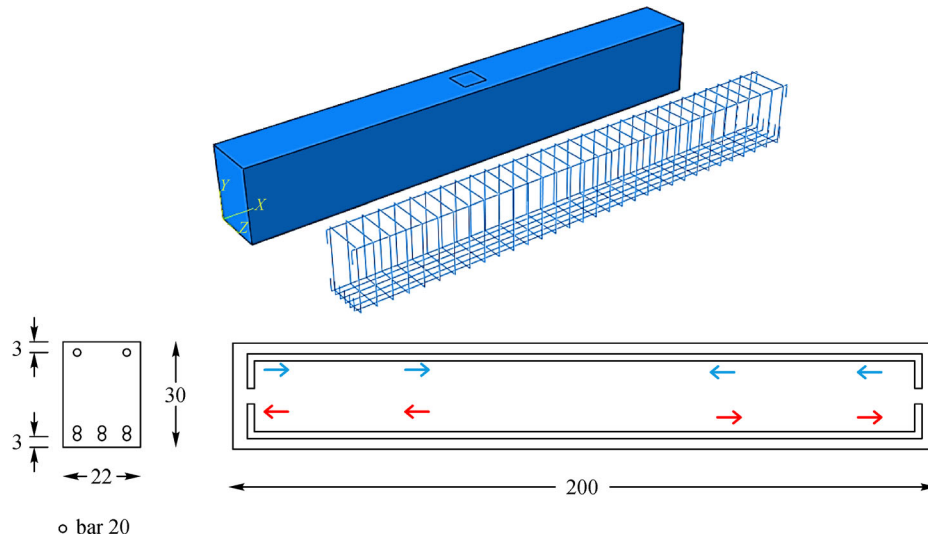
Fig. 1　Common simply supported RC beam with compressive and tensile reinforcement bars (unit: cm).
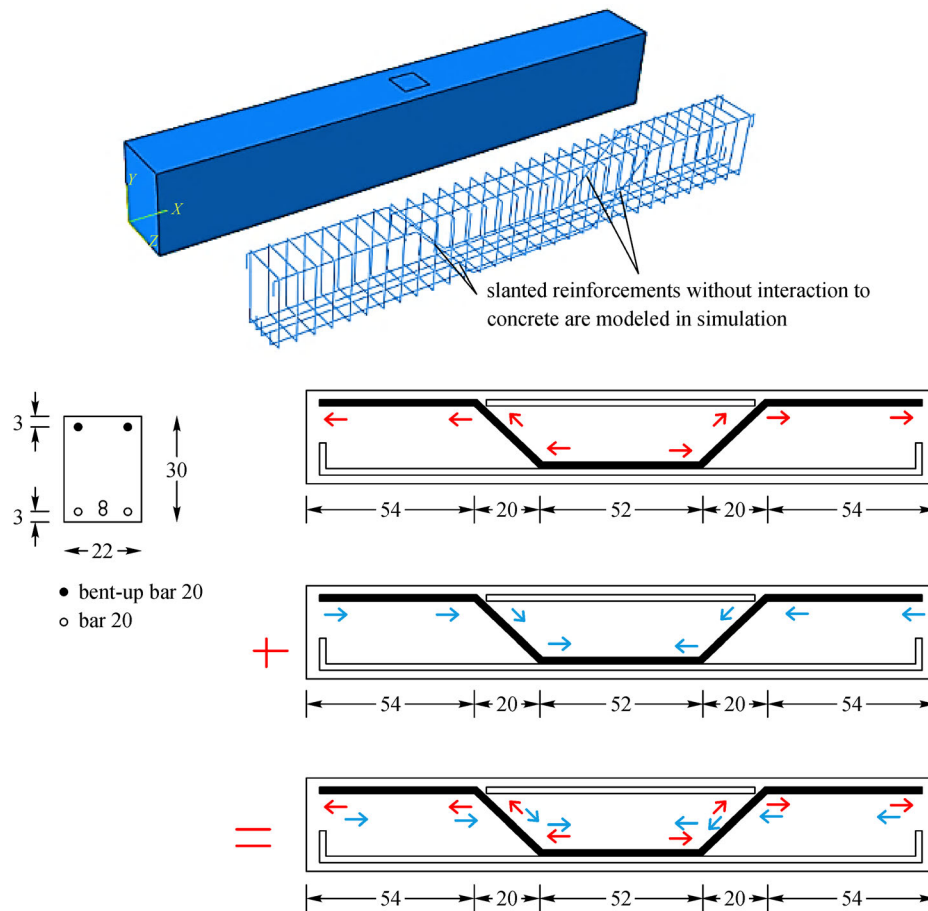

Fig. 2　A superposition of the stress created in the bent-up bars (unit: cm).

guided in the tensile zone at the lower sector of the beam middle-third. Besides, the slanted part of the bent-up bars is placed inside the rubber tube to avoid contact or any interactions with concrete. Thus, bent-up bars represent the bond between the compressive and tensile stresses acting against each other. The superposition method shows that the stress created in the compression zone is transferred to the tensile zone causing a reduction in the tensile stress

created in the mid-beam tensile section. A reverse action also occurs for the tensile stress created in the tensile zone. Figure 2 also shows placement of reinforcement in the simulated model of NRBS. In that model, care was taken for the bent-up bars not to have any interactions with concrete either.

3   Research methodology

To study the accuracy and behavior of the proposed approach, use was made of the FEM simulation, using ABAQUS Software and laboratory test methods. The section form, reinforcement pattern, procedures of the FEM modeling, and the tests/experiments are explained in the following [22].

4   FEM

There are numerous publications regarding the computational modeling of concrete and RC [23–27]; in addition, there are many useful papers on the subject of computational methods for fracture and crack modeling [28–34]. In this study, a 3D FEA model was developed using the ABAQUS commercial software to detail the analysis of the bending performance of the ordinary and the NRBS. The structural behavior of the suggested model is investigated as well. The concrete and the rebar were modeled using 3D solid element and B33 element, respectively, in ABAQUS software. The elastic modulus and Poisson's ratios of the concrete were 30.891 MPa and 0.18, and they were 200 GPa and 0.3 for steel, respectively. The loading was initially classified into the system as the displacement control loading. Simply supported boundary conditions were considered in the test. The plastic model in ABAQUS was used to simulate the nonlinear material behavior of steel as a ductile material. Concerning reinforcement bars, both the elastic and plastic states were considered. Thus, the concrete damaged plasticity model was used for the 30 MPa nonlinear performance of concrete [35]. Tables 1–4 show property of steel and concrete which are modeled in the FEM models. In the ABAQUS software used, the elastic modulus and Poisson's ratio of the steel were selected as 200 GPa and 0.3, respectively; moreover, the behavior of steel was considered as plastic. The stress-strain values of steel reinforcement bars are shown in Table 1.

The elastic modulus and Poisson's ratios of the concrete were selected as 30.891 MPa and 0.18, respectively. The values of concrete damaged plasticity used in the software, are shown in Tables 2–4. It is worth mentioning that to quantify the effectiveness of all input parameters, a sensitivity analysis may be carried as reported by Vu-Bac et al. [36] and Hamdia et al. [37].

The results are based on the Φ20 bars extensometer tests

Table 1   The plastic behavior of the reinforcement bars

yield stress (MPa)	plastic strain
400	0.00%
400	0.03%
450	0.05%
500	0.06%
550	0.07%
600	0.13%
609	0.22%
600	0.24%
550	0.27%

Table 2   The values of concrete damaged plasticity

dilation angle	viscosity parameter	F_{b0}/F_{c0}	K	eccentricity
30	0	1.16	0.67	0.1

Table 3   Tensile behavior of concrete

yield stress (MPa)	cracking strain
2.79	0.00000%
3.10	0.00020%
0.10	0.00042%

Table 4   Compressive behavior of concrete

yield stress (MPa)	inelastic strain
16.32	0.0000%
20.48	0.0008%
24.00	0.0010%
26.88	0.0012%
29.12	0.0014%
29.80	0.0016%
30.90	0.0018%
29.00	0.0022%
26.00	0.0029%
20.00	0.0036%
15.00	0.0043%
6.40	0.0054%

performed at the laboratory. In the steel-concrete interaction modeling, the embedded rigid element model was used and only the slanted part was excluded. The diagonal reinforcement bars of new model (NRBS), located in rubber tube, do not have any contacts with concrete. Therefore, the diagonal parts of reinforcement bars have no interaction such as embedded rigid, tie, etc., with concrete in the FEM model.

Mesh sizes were smaller for steel bars compared to concrete; moreover, the bars was 20 mm (linear) while that

of concrete was 30 mm (cubic). It is noteworthy that the loading was static and nonlinear with respect to time; further, the load was applied on a 100 mm × 100 mm plate at the beam mid-span [38,39].

5 Experimental program

This investigation had a two-step experimental program. In the first step, the material property was specified by stress-strain test. The property of the reinforcement bar and concrete was evaluated by tension and compressive tests respectively. These tests were carried out with standard test methods [40–44]. The second experimental program consists of four 300 mm (d) × 220 mm (w) specimens simply-supported RC beams, having a clear span of 2000 mm, was carried out in the laboratory. The specimens were cast in two series, one traditionally and the other using the new proposed reinforcement pattern (NRBS), which are called ordinary model and new model, respectively. Figure 3 shows reinforcements bars of the ordinary and new models and also rubber tubes (no interaction zone) in the NRBS specimens. To compare the laboratory results and check their accuracy, two beam specimens were made for each model. All specimens were tested under three-point bending. The structural behavior of all beams were observed and monitored during the test by recording vertical displacements and the loads [9,21]. A control machine applied the loading with the same loading speed for all the tests. Loading was increased up to the failure of the specimens. Three linear variable differential transformers (LVDTs) monitored the displacements during the tests. One LVDT was placed at the mid-span of the beam for calculating the maximum displacement and other LVDTs were located at the supports for measuring the opposite direction displacements according to the applied load. The hydraulic jack was placed at a plate (100 mm × 100 mm) and they were located at mid-span of the beam. The hydraulic jack applied the loading at mid-span of the beam. Figure 4 shows the schematic view and original photo of the experimental setup. In return, they demonstrated arrangement of the measurement devices and hydraulic jack presented for the given purpose.

Two beams having common reinforcement pattern were

(a)

(b)

(c)   (d)

Fig. 3 Reinforcements in the ordinary and new models (NRBS). (a) Rubber tubes (no interaction zone) in the new model (NRBS); (b) assembled models; (c) section of assembled models; (d) models before laboratory test.

reinforced with six 20 mm diameter steel bars (reinforce-ment ratio $\rho_s = 0.22\%$) in tension and two 20 mm diameter steel bars in compression. Vertical reinforcement consisted of 10 mm bars at 100 mm spacing (as mentioned before in Fig. 1). Moreover, for the other two beams having the NRBS, four same size bars were positioned in the lower part and two trapezoidal and two compressive bars (to be replaced after the bent part) in the upper portion.

The ordinary and the NRBS specimens were made similar to their finite element counterparts, but before the concrete placement, the bent-up bars were covered with a rubber tube and the two ends were sealed with glue to prevent the concrete from entering the tube (as shown in Fig. 3).

5.1 Material properties

The reinforced bars were of the A-III grade type (400 MPa grade) and underwent the extensometer test. The concrete was of the 37 MPa grade made in a mixer with Portland cement; use was also made of the super plasticizer by an amount equal to 0.5% by weight of the concrete to minimize the formation of air bubbles in the specimens during vibration. The reduction on concrete air bubble, decreases tests errors as well as the standard deviation of the compressive strength. To determine the test-time and the 28-day compressive strength, four 150 mm × 150 mm × 150 mm samples were taken from the concrete of each beam. After placing and vibrating the concrete, the models were kept under similar climatic and temperature condi-tions for the 14-day curing [45].

Next, the cubical specimens were tested in the BHRC structure laboratory under similar loading and boundary conditions; moreover, the concrete compressive test specimens were tested at 28-day age and the mean compressive strength of specimens were nearly 30 MPa and then both, the ordinary and the new models (NRBS) were tested on day 28th.

5.2 Test setup and instrumentation

At the two ends of the beam, roller supports were placed on rigid beds and two deflect-meters (also referred to as LVDTs) were mounted on the beam top, where it rests on the supports, to record the probable support settlement and the more precise mid-span deflection. Further, another deflect-meter was mounted at the middle of the beam. Up to the ultimate bending capacity (end of the elastoplastic state), loading was static (50 kg/s) after which, in the plastic range, it was changed into the displacement type (0.025 mm/s) [21,45].

When the tests started, load-displacement information of mid-span of beam was given to the data logger so as to compare the results (shown as p-Δ curves) with those determined by ABAQUS. Comparisons of the experi-mental and the FEM-based results confirm the accuracy of the proposed theory and modeling [21,35].

6 Results and discussion

One specimen from each FEM and two types of the test models were studied as well as the p-Δ curves. They were drawn to determine each model's bending capacity, strength, and ductility. The bending capacity for the elastic, elastoplastic, and plastic (ultimate limit) states is shown in Fig. 5 using p-Δ curves. In this figure, point B, E, and F specify cracking concrete, yielding stress, and the ultimate limits, respectively [39,45].

Figure 6 shows the results of a comparison between ABAQUS modeling and laboratory test. Figure 6(a) shows the numerical and laboratory results of the ordinary models in p-Δ curves. The laboratory test results are the same as those of the FEM in the ordinary model. Figure 6(b) shows the numerical and laboratory results in p-Δ curves of the new model (NRBS). In the present study, the beams 1 and 4 are referred to as ordinary models and the beams 2 and 3,
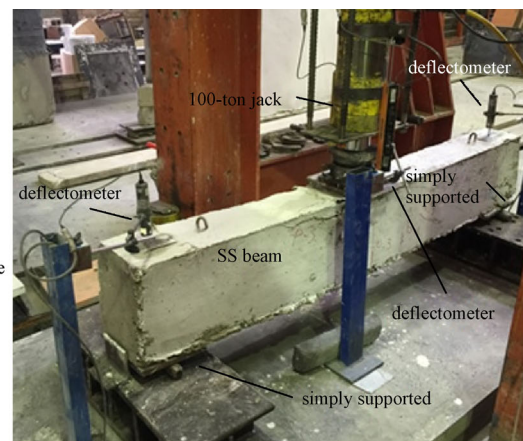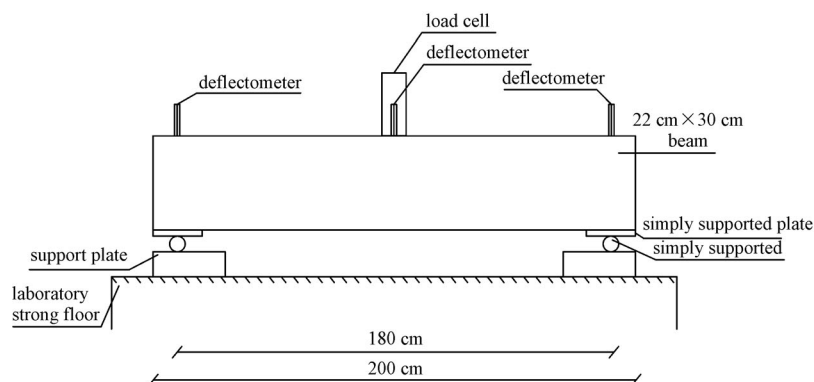

Fig. 4 Details of the tested beam below a 100-ton jack and location of the deflect-meter.
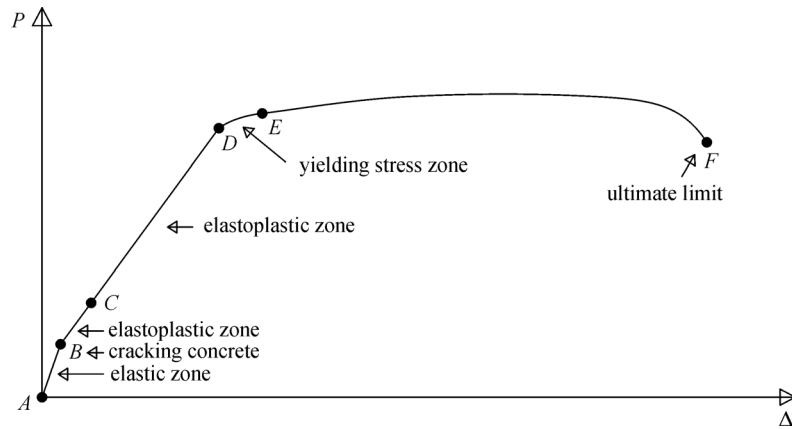
Fig. 5 Elastic and elastoplastic, ultimate limit, cracking concrete and yielding stress state in p-Δ curves [45].
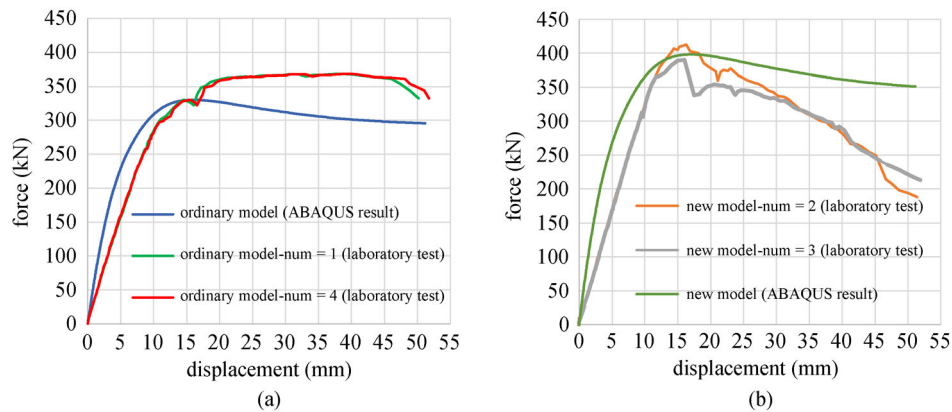

Fig. 6 (a) Verification of ordinary model in laboratory test and ABAQUS p-Δ curve; (b) verification of new model (NRBS) in laboratory test and ABAQUS p-Δ curve [39].

built by NRBS, are addressed as new models. The bending capacity of beams 1 and 4 in yield stress state were recorded 293.57 and 316.71, respectively, and the strength of beams 2 and 3 were noted more as 413.02 and 398.34, respectively, in yield stress state. As a result, the bending capacity in the yield stress zone of the new model (NRBS) were shown as 34% increase, as shown in Fig. 6.

The bending capacity is decreased in the new model (NRBS) after the yield stress zone, which is shown in p-Δ curves. Decreasing bending capacity occurs after the state of yield stress because stress concentration is very high in the rubber tube zone as shown in the laboratory test results of Fig. 6. The lowest shearing capacity is evident at this zone. Hence, progressive failure occurs after yield stress state in new models (NRBS). The p-Δ results of the new model laboratory tests show that after 34% increase, the bending capacity starts to decrease due to the area reduction (where steel and concrete separate); and beam shear capacity reduction in this part is due to the excessive loading.

Figure 7 performs the p-Δ of laboratory test results for a more precise comparison of the two models. As a result, although the bending capacity and strength is increased in the new models (NRBS) up to the yield stress state, the ductility of new models (NRBS) are lower than the ordinary models [39].

In laboratory test program, four beams are tested, which two of them are ordinary beam (the beams 1 and 4). The beams 2 and 3 are built by the NRBS. The p-Δ results of laboratory tests are shown in Fig. 7. These results are explained the moment capacity of beams.

The bending capacity of the new model (NRBS) is 32.31% more than that of the ordinary model in the state of yield stress as shown in the ABAQUS observation. As a result, the p-Δ results in both the FEM and the laboratory tests under static analyses show that the bending capacity of the new model (NRBS) is more than that of the ordinary model in the state of yield stress but the bending capacity of NRBS models decrease after the state of yield stress. The shear resistant of new model (NRBS) was not apparent against excessive loading in the section with rubber tubes, because the shear cracks were expanded next to the
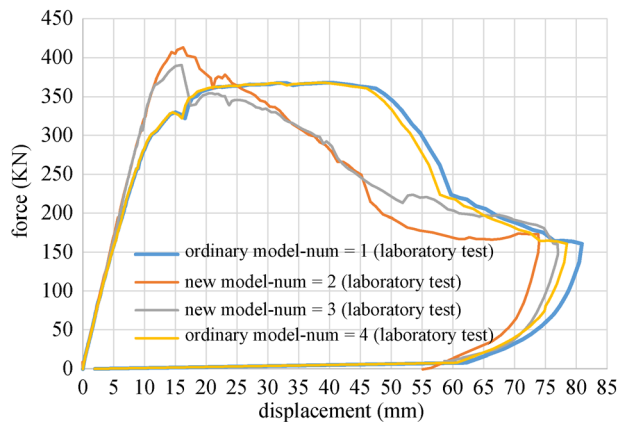
Fig. 7 The p-Δ curves of New and ordinary models (laboratory tests results).

applying excessive loading. Thus, the failure occurred because of expanding shear cracks as shown in the laboratory tests [39]. As a consequence, the new models (NRBS) do not have sufficient ductility as shown in Fig. 7. The laboratory tests result show that after the ordinary beam reaches its yield stress strength, it continues experiencing displacement with the same strength as nearly four times. Regarding the new model, there is a shear failure in the section with rubber tube; the specimen seems more brittle because loading is 34% higher (than ordinary beam) and the shear capacity is weak in the rubber tube vicinity. The reason can also be the mid-span concentrated loading of 1.34 times that of the ordinary beam, which has caused more shear and normal stress concentration at the mid-span, and the occurrence of brittle failure [39,45].

Table 5 shows bending capacity of beams in three situations, which are the crack beginning state (ending elastic behavior of beams), yielding stress state (the bottom

longitudinal steel bars were yielded), and the ultimate limit state. The mean bending capacities of the new models were 55.2%, 32.31%, and 18.85% more than the corresponding mean bending capacities in respective states of crack initiation, yield stress and ultimate limit states. The results of the bending capacity of beams are valid in the state of the ultimate limit.

A comparison of the p-Δ results found by laboratory tests and the FEM by the starting point up to the ultimate bending capacity where the tensile reinforcement reaches its yield point reveals that the results are acceptable. After the yield point up to the maximum plastic bending capacity, the results somewhat diverge because of the fact that the concrete crack zone is considered continuous in the FEM software; moreover, the mid-span reinforcement bars reach their maximum plastic stress in the tensile zone. Under static displacement loading and after the bar stress reaches its ultimate value, the reduced part of the bar stress-strain curve becomes negligible and the calculations are stopped.

As shown in Table 5, the first beam, as the ordinary one, started cracking when the load and bending moment were 52.2 kN and 24.79 kN·m, respectively. This load was 16.15% of the ultimate load. When the tension reinforcement bars were yielded, the load and bending moment were 293.57 kN and 139.45 kN·m and in ultimate limit state, the load and bending moment were 323.4 kN and 153.92 kN·m, respectively. The fourth beam in Table 5, as the second ordinary one, starts cracking when the applied load reached 57.8 kN and the bending moment was 27.45 kN·m. As observed in the experimental test, this beam was in elastoplastic state until the load reached 316.71 kN and the ultimate state was observed when load reached 329.2 kN. Therefore, the bending moment was 150.44 and 156.37 kN·m in yield stress and ultimate state, respectively, as shown in Table 5.

Table 5 Bending capacity at the start of crack, yielding stress and ultimate limit state

no.	model	state	bending capacity (FEM result) (kN·mm)	load (kN)	bending capacity (laboratory result) (kN·mm)
1	the first sample of ordinary model	crack beginning	24588	52.20	24795
		the state of yield stress	146412	293.57	139446
		the state of ultimate limit	140369	323.40	153615
2	the first sample of new model	crack beginning	38135	88.90	42228
		the state of yield stress	193720	423.80	201305
		the state of ultimate limit	166883	339.04	161044
3	the second sample of new model	crack beginning	38135	82.60	39235
		the state of yield stress	193720	393.50	186913
		the state of ultimate limit	166833	314.84	149530
4	the second sample ordinary model	crack beginning	24588	57.80	27455
		the state of yield stress	146412	316.71	150437
		the state of ultimate limit	140369	329.20	156370

The second and third beams were built by the new NRBS model. The first crack in second beam was appeared as a flexural crack when the load and the bending moment reached 88.9 kN and 42.23 kN·m as shown in the experimental test. The tension reinforcement bars of the second beam were yielded when the load was 423.8 kN. Afterwards, the expanding shear cracks were further increased because it was overloaded and recorded more than the shear capacity of the beam. Hence, bending capacity of the beam was decreased after the yield stress state which led to failure. In addition, the second beam was failed, when the load was 339.04 kN. Therefore, the bending moment was 201.31 and 161.04 kN·m in yield stress and the ultimate state, respectively. In the third beam, the first crack was created when the load was 82.6 kN and the bending moment was 39.24 kN·m in this state as shown in Table 5. When the load reached 393.5 kN, the reinforcement bars yielded, and its bending capacity was decreased which then led to failure. When the load was 314.84 kN, the third beam failed. In addition, the bending moment was 186.9 and 149.53 kN·m in yield stress and the ultimate state, respectively.

Figure 8 shows cracking in the beginning crack state, yield stress state and the ultimate limit state for the new and ordinary models in the laboratory test. Bending cracking is created in mid-span of the beams. Figures 8(a), 8(c), and 8(e) show the cracking of the ordinary beam on state of the elastic zone, elastoplastic zone, and state of ultimate limit, respectively. In addition, the cracks on the new model (NRBS) are shown in Figs. 8(b), 8(d), and 8(f), representing the state of the elastic, elastoplastic, and the ultimate limit, respectively.

Based on the above data, the first crack appeared as a flexural crack when the loads were 52.2 and 57.8 kN in ordinary beams as shown in the laboratory tests. Furthermore, the first cracks appeared as a flexural crack when the loads were 82.6 and 88.9 kN in new model beams as shown in the laboratory tests. Then some flexural cracks were created on mid-span of the beams by extra loading that are shown in Figs. 8(a) and 8(b). Before the bending crack (first crack) was created, the beam exhibits elastic behavior. It is specified that cracks are created on mid-span of the beam in the crack beginning state that all were created through stress due to bending moment. The cracks were created on mid-span of the beam next to the crack of the beginning state until the state of yield stress, which all are vertical. Figures 8(c) and 8(d) show the ordinary beam and the new model beam (NRBS), respectively, when the state of these beams was in yield stress. In this state, all the cracks were vertical and their intensity on the new model beam were more than the cracks on ordinary beam. The distance of the vertical cracks on the new model were less than the vertical cracks on ordinary beam as shown in Figs. 8(c) and 8(d). The longitudinal steel reinforcements of ordinary beams were yielded at 293.57, 316.71 kN and at 10.88, 10.75 mm displacements, respectively. In addition,

the longitudinal steel reinforcements of new model beam were yielded at 423.8, 393.5 kN and at 11.97, 12.99 mm displacement, respectively. The shear cracks are created during the state of the yield stress, being diagonal many of which are shown under the jack and upper simple supports. The expansion of diagonal cracks is increased until the ultimate limit state. This situation occurred in new model beams earlier than ordinary beams because the applied load at the new model beam was overloaded. Figure 8(e) shows the vertical cracks in mid-span of beam which were increased in ordinary models and the expanding vertical cracks were the reason of failure in ordinary models. Figure 8(f) shows the failure state of new model beams. In the state of ultimate limit, the expansion of diagonal crack (shear cracking) is propagated under the jack up to the simple supports and it causes failure in the new models [46–48].

Figure 9 shows stress contour of the concrete in ordinary beam and the new model beam. These stresses were calculated by the FEM analysis. It was carried out by ABAQUS software [39]. According to Tables 3–4, the maximum experimental compressive and tension stress of concrete were recorded as 30 and 3 MPa, respectively, being therefore those of the crack limit. Figure 9 shows cracks with gray color in the same zone that the laboratory tests were shown in Fig. 8. Figures 8 and 9 show similar zone cracking in each state through comparison between simulation and the experimental results. Thus, it ensures validation of the present research. In addition, the gray color zone in Figs. 9(a) and 9(b) is the region where the tensile stress of concrete is greater than 3 MPa. The ordinary beam exhibits elastic behavior when the load reaches 49.167 kN using FEM, whereas the new model beam has elastic behavior with the load recorded 70.27 kN. Similar to the laboratory test in Figs. 9(a) and 9(b), it is shown that early cracks are created in mid-span of beams and all the cracks are of the bending moment type. The FEM and laboratory results indicate that the start of cracks are located in the lower zone of the neutral surface in mid-span of the beam.

The beams had elastoplastic behavior when the area of crack was increased at beams. When the reinforcement bars were yielded, the elastoplastic state was ended. The steel bars were yielded in extensometer experimental test when the tensional stress of steel bar was 400 MPa. Therefore, the reinforcement bars were yielded in the FEM result when the stress of longitudinal steel reinforcements were reached 400 MPa. First, the longitudinal steel reinforcements placed under natural axis reached 400 MPa in all beams. The longitudinal steel reinforcements of ordinary beam were yielded at 292.82 kN and 10.99 mm displacement in the FEM result. In addition, the longitudinal steel reinforcements of new model beam were yielded at 387.44 kN and 12.03 mm displacement. When steel bars were yielded, other crack zones were created under the jack plate and at the top of the simple supports as
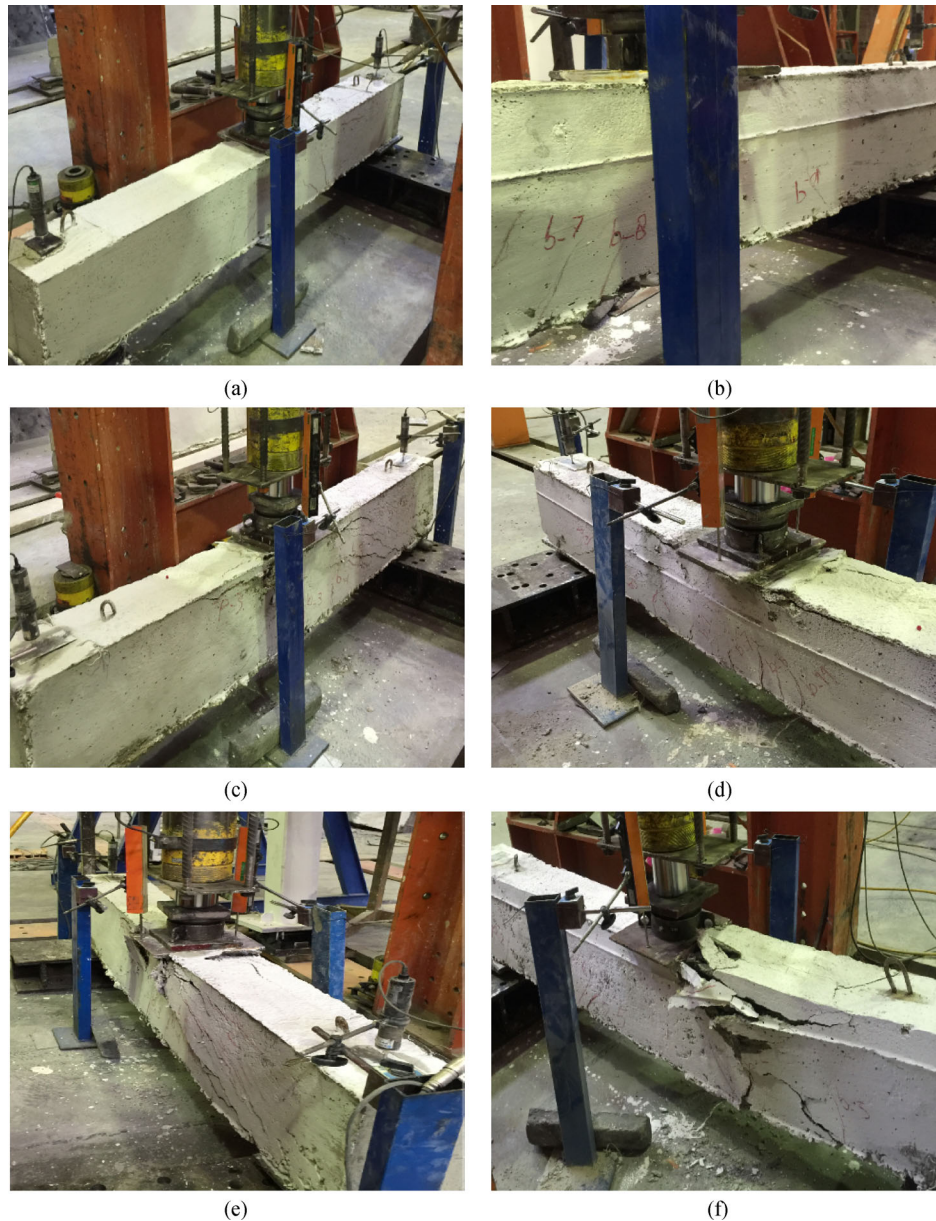
(a)

(b)

(c)

(d)

(e)

(f)

Fig. 8 Laboratory test results. (a) Crack beginning in the ordinary model; (b) crack initiated in the new model (NRBS); (c) the ordinary model cracking in the state of yield stress; (d) the new model (NRBS) cracking in the state of yield stress; (e) the ordinary model cracking in the state of ultimate limit; (f) the new model (NRBS) cracking in the state of ultimate limit.

shown in Figs. 9(c) and 9(d). Furthermore, the laboratory tests were performed in the same locations of the cracks in the state of yield stress as presented in Figs. 8(c) and 8(d). These new crack zones were created by compressive stress and are shown by black color in Figs. 9(c) and 9(d). Next, the beams had plastic behavior along with excessive load. In fact, the FEM and the laboratory results show that the locations of cracks are the same. The diagonal cracks were created during plastic behavior of the beams. When the beams failed, the diagonal crack zone was increased and covered the maximum area during beam analysis, as shown in Figs. 9(e) and 9(f). The ultimate loads were 280.64 and 333.67 kN for ordinary and the new model

beams, respectively. The diagonal cracks were created because concentration stress under the jack, at the top of the simple supports and in the bent-up bars were increased in this state; therefore, the expansion diagonal cracks are increased after the state of yield stress. In addition, the cracks are created in compressive section (up to the natural axis) and tension section (below the natural axis) by 30 and 3 MPa stress, respectively, using the FEM model. As shown in Figs. 9(e) and 9(f), the expansion of cracks is increased by more than 30 MPa in the compressive stress. One realizes that the area of the cracks zone in the new model beam is larger than the ordinary model. In addition, it is specified that diagonal cracks are improved in the state
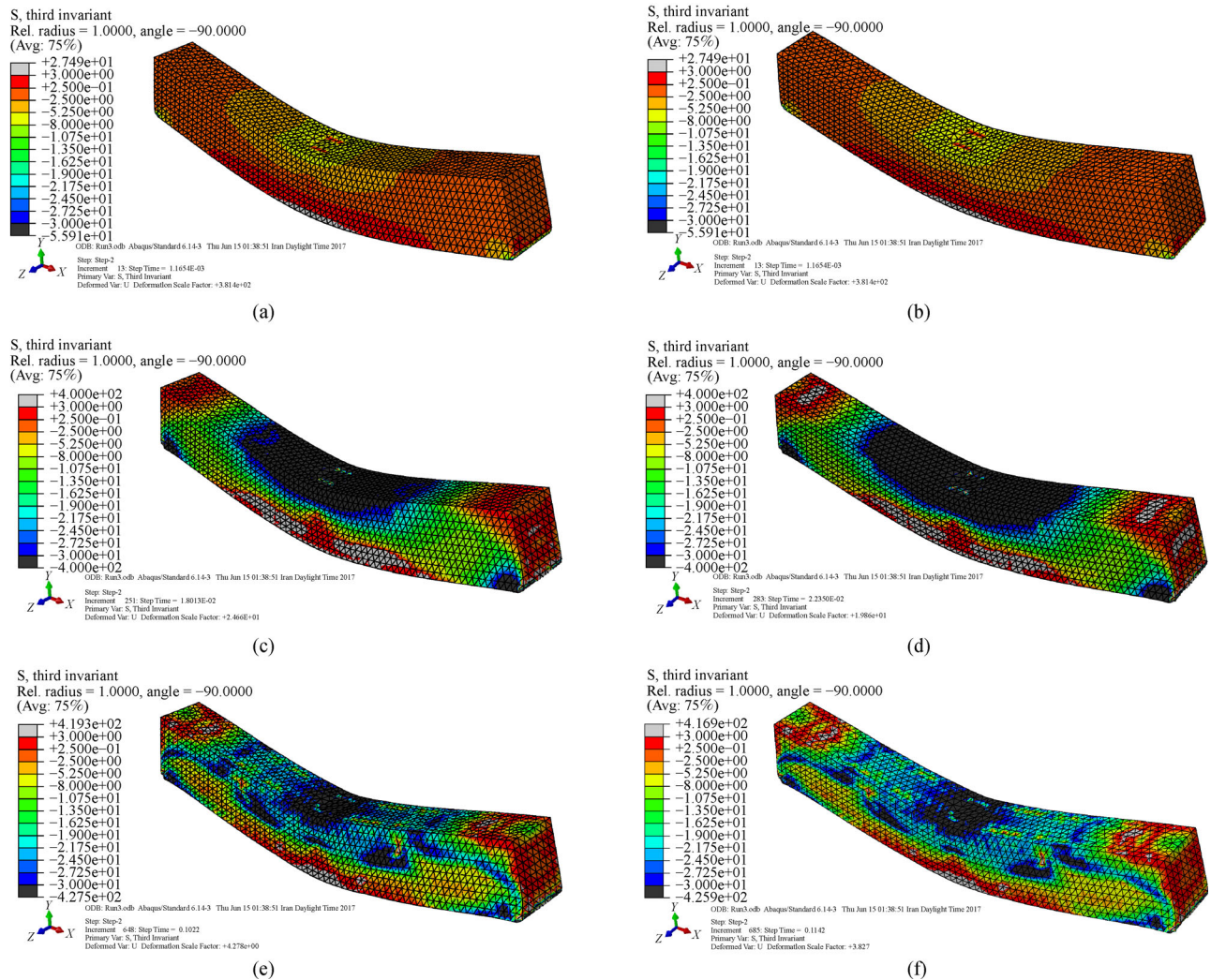
Fig. 9 ABAQUS simulation results. (a) Ordinary model at the early state of crack launching; (b) new model cracking at the early state of crack launching; (c) ordinary model cracking in the state of yield stress; (d) new model cracking in the state of yield stress; (e) ordinary model cracking in the state of ultimate limit; (f) new model cracking in the state of ultimate limit.

of the ultimate limit [39]. Figures 8(e) and 8(f) show cracks of ordinary and the new model in the state of ultimate limit; in addition, Figs. 9(e) and 9(f) show the location of cracks of ordinary and the new model in the state of ultimate limit. These figures show the location of crack in the laboratory and the FEM results which are the same in the state of ultimate limit.

Figure 10 shows the stresses of the reinforcement bars of the ordinary beam and the new beam in the state of yield stress bending capacity. Figure 10(a) illustrates some compressive and tensile stresses created above and below the neutral axis of a beam section, respectively. Figure 10(b) displays enforced tension stress to compressive (upper beam) by no interaction of reinforcement. The new model beam is used from the maximum tension and compressive capacity of longitudinal steel reinforcements

when the bottom reinforcement bars are yielded as shown in Fig. 10(b) [39].

Figure 11 shows PEEQ in ordinary and the new models. The PEEQ refers to the equivalent plastic strain in ABAQUS [39]. Figure 11(a) shows failure cracks created under the jack plate and at the top of the simple supports. It behaves similar to the laboratory results in ordinary beam. Figure 11(b) shows failure cracks which are created in midspan on new model beam and under the jack plate and at the top of the simple supports. The results show that failure cracks occur at the same location as in the laboratory and the simulation results. Another words, shape and zone of the cracking and the failure cracking in the laboratory test have the same shape and zone in the simulation result. For example, the result of the Fig. 11(a) validated Fig. 8(e) and both figures present failure cracking in the ordinary
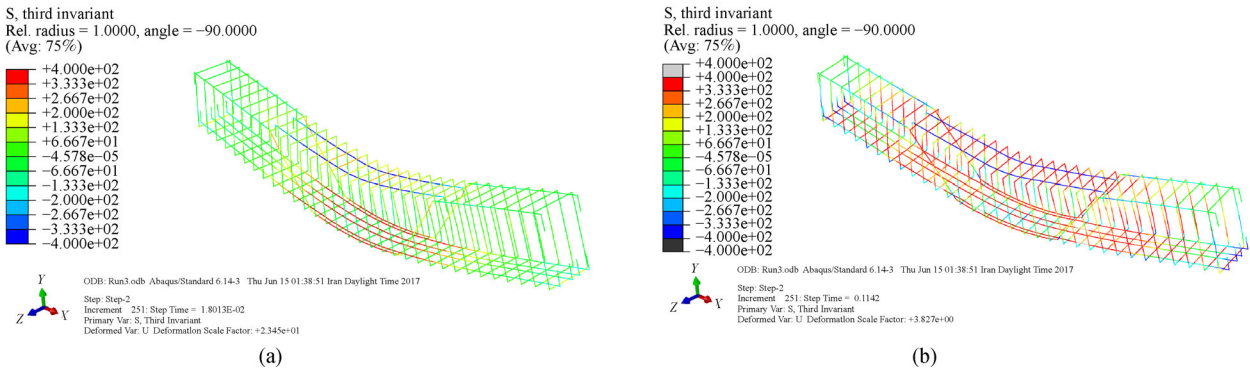
(a)   (b)

Fig. 10   (a) Ordinary model reinforcement bar stresses in the state of yield stress; (b) new model reinforcement bar stresses in the state of yielding stress [39].
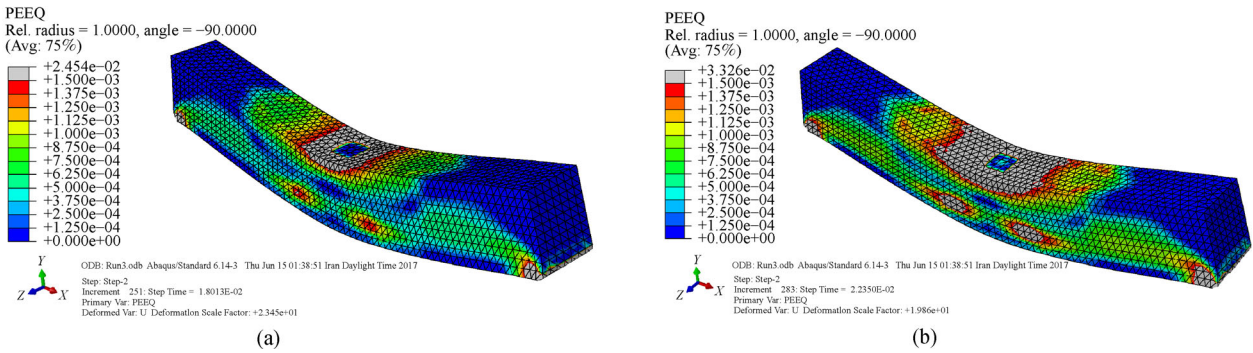

(a)   (b)

Fig. 11   (a) Equivalent plastic strain in ordinary model; (b) equivalent plastic strain in the new model [39].

model. In addition, the area of plastic strain on the new model beam is larger than ordinary model. In addition, the failure cracking is created under the jack plate and upper simple supports in the ordinary model, which are continued by diagonal cracks similar to the laboratory results. Figures 11(b) and 8(f) show the same cracking zone, and both show failure cracking in the new model. Failure cracking is created under the jack plate and the simple supports which is continued by diagonal cracks. In addition, a large failure zone is created on these diagonal lines, which are shown in Figs. 11(b) and 8(f). This zone is specified with gray colored circle in Fig. 11(b) [39].

7   Formula for calculating bending capacity of NRBS

As the first step, it should be specified whether the upper and bottom longitudinal steel reinforcements are yielded or not. As observed, the bottom and upper reinforcement bars of the new model and ordinary beams are yielded in mid-span of beams. If the bottom and upper longitudinal steel reinforcements are yielded, the mathematical form of bending capacity of the RC beam is formulated as:

$$M_{\mathrm{n}} = \left(A_{\mathrm{s}} \times f_{\mathrm{y}} - A'_{\mathrm{s}} \times f'_{\mathrm{y}}\right)$$
$$\times \left(d - \frac{a}{2}\right) + A'_{\mathrm{s}} \times f'_{\mathrm{y}}(d - d'), \tag{1}$$

$$a = \frac{A_{\mathrm{s}} \times f_{\mathrm{y}} - A'_{\mathrm{s}} \times f'_{\mathrm{y}}}{0.85 \times f'_{\mathrm{c}} \times b}, \tag{2}$$

where M_{n} is the bending capacity of beam; a is the length of the depth of beam, which is called length of Whitney equivalent rectangular stress; b, d, and d' are width, upper and under cover of beam, respectively; f'_{c} is the maximum compressive stress, causing concrete to fail under; f_{y} is the maximum tension or compressive stress of the longitudinal steel reinforcement, causing steel bar to yield, f'_{y} is the compressive stress experienced by the upper longitudinal steel bar under bending capacity and it is 400 in the ordinary beam. The numerical bending capacity of ordinary beam is 124.3 kN·m. On the other hand, when the load is 248.56 kN, the moment of ordinary beam reaches its bending capacity. Moreover, the mean of bending capacity of beams is 152.1 kN·m in yield stress state; therefore, the safety factor of numerical bending capacity of ordinary beams are 1.22 in present study [47,48].

First, for calculation of bending capacity of the new model beam (NRBS), the force of upper longitudinal steel reinforcements should be calculated at 1/3 of the new model beam (NRBS). Afterwards, this force should be reduced from bottom longitudinal steel reinforcements at mid-span of this beam. The bottom reinforcement bars of the new model beams are yielded at 1/3 of the beam spans as calculated by Eq. (3). Another way of calculating the bending capacity of this beam is by superposition, as explained in Section 2 of this paper. Equation (4) is derived from Eq. (2) by superposition. a' is calculated for mid-span of new model beam. It is specified that amount of a' is more than a at Eq. (2), because there is extra positive parameter in Eq. (4):

$$a = \frac{A_s \times f_y - A'_s \times f'_s}{0.85 \times f'_c \times b}, \tag{3}$$

$$a' = \frac{A_s \times f_y - A'_s \times f'_y + A'_s \times f'_s}{0.85 \times f'_c \times b}, \tag{4}$$

where f'_s is the stress of the upper longitudinal steel reinforcements at one third of the beam length. This section acts similar to an ordinary beam. Thus, the force of the upper longitudinal steel reinforcements is calculated easily. f'_s can be calculated by moment, which is present at 1/3 of the beam. Therefore the formula of f'_s is given by:

$$f'_s = \frac{2}{3} \times \frac{400 \times (a - 0.85 \times d')}{a} < f'_y. \tag{5}$$

In this problem, a is 70.9 mm and f'_s is 166.65 MPa and the force of the upper longitudinal steel reinforcement is 104.65 kN. Therefore, the amount of a' is 108.14 mm but amount of a is 70.9 mm in ordinary beam. The mathematical form of bending capacity of new model beam is formulated as:

$$M_n = 0.85\left(A_s \times f_y - A'_s \times f'_y + A'_s \times f'_s\right)$$
$$\times \left(d - \frac{a}{2}\right) + A'_s \times f'_y(d - d'). \tag{6}$$

The bending capacity M_n was determined to be 162.7 kN·m. as calculated by Eq. (6). Thus, when the load is 325.4 kN, the moment of the new model beam reaches the bending capacity. Therefore, the mean of bending capacity of the new model beam is 1.20 times more than the bending capacity calculated by Eq. (6).

The bending capacity of new model is 0.30% more than bending capacity of ordinary beam in this evaluation (evaluate by formula). The mean of safety factor for calculation of bending capacity of ordinary beam is 1.22 and the bending capacity of new model beam is calculated by the Eq. (6), which the mean of safety factor of this equation is 1.2 for bending capacity of the new model

beam in this investigation. The result shows these equations are calculated by reliable moment capacity.

8 Conclusions

This paper introduces a new bent-up bars system, which is placed in rubber tube and is called the NRBS in the present study. This bent-up bars can transfer the compressive stress to the tensile reinforcement for the strengthening of the tensile section. In this study, the increasing bending capacity of simply supported beams are evaluated by the FEM and the experimental model. The results showed that using the NRBS for strengthening the beam is not adequate because this system does not have sufficient ductility in plastic behavior. As a result, increasing bending capacity was observed during elastoplastic behavior of the new model. Thus, the bending capacity was increased in the new models until the bottom and upper longitudinal steel reinforcements were yielded. After the yield stress state, when the extra load was applied on the new beam model, its shear capacity was recorded less than the existing load (the stress due to shear force); therefore, the shear crack was created and expanded on the experimental specimen, which eventually it caused failure of the new model.

Some further achievements of the present study are explained as follows:

1) In this investigation, the experimental results of the proposed model were provided and based on the FEM analysis, the results were compared and evaluated. The results show that overlapping of the load-displacement diagrams for the new proposed models has confirmed 34% increase in the bending capacity.

2) This technique, which improved the bending capacity of the new model, is built easily and cheaply. There is no need for specific materials to be used.

3) The FEM analysis of the new model NRBS also confirms greater compressive and tensile capacity of longitudinal steel reinforcements.

4) The FE analyses and laboratory tests show the same locations of cracks at its first propagation, yield stress state and at the ultimate limit zone.

5) In addition, the increasing area of the bending cracks in the beam web, conforms the results conducted from the load-displacement diagrams of the laboratory tests and those of the FEM Software. They all indicate that the stress transfer theory is valid.

6) The proposed technique showed that increasing bending capcaity is possible through transferring the stress from compressive reinforcement to tensile reinforcement; however, it is not recommended for increasing shear capacity, bearing capacity and ductility.

7) The cross sectional area of NRBS in bent-up reinforcement bar is less than other cross sections in this model due to the presence of rubber tubes. Thus, these areas are weakned and the shear cracks were created in

these sections and expanded therefrom. Subsequently, expansion of diagonal cracks in bent-up reinforcement area caused the new beams to fail.

8) The bending capacity formula of the ordinary beam is developed by superposition method in order to determine an equation to calculate the bending capacity of the new model.

9) The mean safety factors of bending capacity of the ordinary and the new model beams were found to be 1.22 and 1.2, respectively showing the fact that the formula for calculating bending capacity is reliable.

10) The new model beams did not have sufficient ductility. To improve such weakness, increasing shear reinforcements may be suggested.

References

1. Figeys W, Verstrynge E, Brosens K, Van Schepdael L, Dereymaeker J, Van Gemert D, Schueremans L. Feasibility of a novel system to prestress externally bonded reinforcement. Materials and Structures, 2011, 44(9): 1655–1669

2. Kotynia R, Cholostiakow S. New proposal for flexural strengthening of reinforced concrete beams using CFRP T-shaped profiles. Polymers, 2015, 7(11): 2461–2477

3. Papanicolaou C G, Triantafillou T C, Papathanasiou M, Karlos K. Textile reinforced mortar (TRM) versus FRP as strengthening material of URM walls : Out-of-plane cyclic loading. Materials and Structures, 2007, 41(1): 143–157

4. Pham T M, Hao H. Review of concrete structures strengthened with FRP against impact loading. Structures, 2016, 7: 59–70

5. Tanarslan H M. Flexural strengthening of RC beams with prefabricated ultra high performance fibre reinforced concrete laminates. Engineering Structures, 2017, 151: 337–348

6. Rasheed H A, Abdalla J, Hawileh R, Al-tamimi A K. Flexural behavior of reinforced concrete beams strengthened with externally bonded Aluminum Alloy plates. Engineering Structures, 2017, 147: 473–485

7. Wobbe E, Silva P, Barton B L, Dharani L R, Birman V, Nanni A, Alkhrdaji T, Thomas J, Tunis G. Flexural capacity of RC beams externally bonded with SRP and SRG. In: Proceedings of Society for the Advancement of material and Process Engineering 2004 Symposium, 2004, 16–20

8. Esfandiari M J, Rahimi Bondarabadi H, Sheikholarefin S, Dehghan Manshadi S H. Numerical investigation of parameters influencing debonding of FRP sheets in shear-strengthened beams. European Journal of Environmental and Civil Engineering, 2018, 22(2): 246–266

9. Oehlers D J. Reinforced concrete beams with plates glued to their soffits. Journal of Structural Engineering, 1992, 118(8): 2023–2038

10. Daly A F, Witarnawan W. Strengthening of bridges using external post-tensioning. In: International Conference of the Eastern Asia Society for Transportation Studies, 1997

11. Altun F. An experimental study of the jacketed reinforced-concrete beams under bending. Construction & Building Materials, 2004, 18(8): 611–618

12. Chaallal O, Nollet M J, Perraton D. Strengthening of reinforced concrete beams with externally bonded fiber-reinforced-plastic plates: design guidelines for shear and flexure. Canadian Journal of Civil Engineering, 1998, 25(4): 692–704

13. Smith S T, Teng J G. FRP-strengthened RC beams. I: Review of debonding strength models. Engineering Structures, 2002, 24(4): 385–395

14. Ross C A, Jerome D M, Tedesco J W, Hughes M L. Strengthening of reinforced concrete beams with externally bonded composite laminates. Structural Journal, 1999, 96(2): 212–220

15. Urgessa G S, Esfandiari M. Review of polymer coatings used for blast strengthening of reinforced concrete and masonry structures. In: International Congress on Polymers in Concrete (ICPIC 2018), 2018, 713–719

16. Lee H Y, Jung W T, Chung E. Flexural strengthening of reinforced concrete beams with pre-stressed near surface mounted CFRP systems. Composite Structures, 2017, 163: 1–12

17. Seraj S M, Kotsovos M D, Pavlović M N. Compressive-force path and behaviour of prestressed concrete beams. Materials and Structures, 1993, 26(2): 74–89

18. Shatarat N, Katkhuda H, Abdel-Jaber M, Alqam M. Experimental investigation of reinforced concrete beams with spiral reinforcement in shear. Construction & Building Materials, 2016, 125: 585–594

19. Yang K H, Kim G H, Yang H S. Shear behavior of continuous reinforced concrete T-beams using wire rope as internal shear reinforcement. Construction & Building Materials, 2011, 25(2): 911–918

20. Karayannis C G, Chalioris C E. Shear tests of reinforced concrete beams with continuous rectangular spiral reinforcement. Construction & Building Materials, 2013, 46: 86–97

21. Ghasemi M R, Shishegaran A. Role of slanted reinforcement on bending capacity SS beams. Vibroengineering PROCEDIA, 2017, 11: 195–199

22. Dassault Systems Simulia Corp. ABAQUS Analysis User's Manual 6.10-EF, 2010

23. Rabczuk T, Zi G, Bordas S, Nguyen-Xuan H. A simple and robust three-dimensional cracking-particle method without enrichment. Computer Methods in Applied Mechanics and Engineering, 2010, 199(37–40): 2437–2455

24. Rabczuk T, Belytschko T. Cracking particles: A simplified mesh free method for arbitrary evolving cracks. International Journal for Numerical Methods in Engineering, 2004, 61(13): 2316–2343

25. Rabczuk T, Zi G, Bordas S, Nguyen-Xuan H. A geometrically nonlinear three dimensional cohesive crack method for reinforced concrete structures. Engineering Fracture Mechanics, 2008, 75(16): 4740–4758

26. Rabczuk T, Belytschko T. Application of particle methods to static fracture of reinforced concrete structures. International Journal of Fracture, 2006, 137(1–4): 19–49

27. Rabczuk T, Belytschko T. A three dimensional large deformation meshfree method for arbitrary evolving cracks. Computer Methods in Applied Mechanics and Engineering, 2007, 196(29–30): 2777–2799

28. Ghorashi S S, Valizadeh N, Mohammadi S, Rabczuk T. T-spline based XIGA for fracture analysis of orthotropic media. Computers

& Structures, 2015, 147: 138–146

29. Amiri F, Anitescu C, Arroyo M, Bordas S P A, Rabczuk T. XLME interpolants, a seamless bridge between XFEM and enriched meshless methods. Computational Mechanics, 2014, 53(1): 45–57

30. Areias P, Msekh M A, Rabczuk T. Damage and fracture algorithm using the screened Poisson equation and local remeshing. Engineering Fracture Mechanics, 2016, 158: 116–143

31. Areias P, Rabczuk T. Steiner-point free edge cutting of tetrahedral meshes with applications in fracture. Finite Elements in Analysis and Design, 2017, 132: 27–41

32. Areias P, Reinoso J, Camanho P P, César de Sá J, Rabczuk T. Effective 2D and 3D crack propagation with local mesh refinement and the screened Poisson equation. Engineering Fracture Mechanics, 2018, 189: 339–360

33. Ren H, Zhuang X, Rabczuk T. Dual-horizon peridynamics: A stable solution to varying horizons. Computer Methods in Applied Mechanics and Engineering, 2017, 318: 762–782

34. Ren H, Zhuang X, Cai Y, Rabczuk T. Dual-horizon Peridynamics. International Journal for Numerical Methods in Engineering, 2016, 108(12): 1451–1476

35. Jankowiak T, Lodygowski T. Identification of parameters of concrete damage plasticity constitutive model. Foundations of Civil and Environmental Engineering, 2005, 6(1): 53–69

36. Vu-Bac N, Lahmer T, Zhuang X, Nguyen-Thoi T, Rabczuk T. A software framework for probabilistic sensitivity analysis for computationally expensive models. Advances in Engineering Software, 2016, 100: 19–31

37. Hamdia K M, Silani M, Zhuang X, He P, Rabczuk T. Stochastic analysis of the fracture toughness of polymeric nanoparticle composites using polynomial chaos expansions. International Journal of Fracture, 2017, 206(2): 215–227

38. Andersson S, Karlsson H. Structural response of reinforced concrete beams subjected to explosions, time dependent transformation factors, support reactions and distribution of section forces. Thesis for the Master's Degree. Chalmers: Chalmers University of Technology, 2012, 6–110

39. FEA. Finite Element Analyses. Abaqus/CAE version 6.13: Computer Aided Engineering. Dassault Systemes, 2013

40. ASTM S. Standard Specification for Deformed and Plain Carbon-Steel Bars for Concrete Reinforcement. 615/A 615M-09b, 2009

41. ASTM C. Standard Test Method for Flexural Strength of Hydraulic-Cement Mortars. C348-18, 2018

42. RCSC Committee. Specification for Structural Joints Using ASTM A325 or A490 Bolts. American Institute of Steel Construction (AISC), 2004

43. ASTM C. Standard Test Method for Flow of Hydraulic Cement Mortar. C1437, 2007

44. ASTM C. Standard test method for compressive strength of cylindrical concrete specimens. C39/C39M-12, 2012

45. Iribarren B S. Progressive collapse simulation of reinforced concrete structures: Influence of design and material parameters and investigation of the strain rate effects. Dissertation for the Doctoral Degree. Brussel: Université Libre de Bruxelles, 2011

46. Schlaich J, Schäfer K, Jennewein M. Toward a consistent design of structural concrete. PCI Journal, 1987, 32(3): 74–150

47. ACI Committee. Qualification of post-installed mechanical anchors in concrete and commentary. ACI Comm, ACI 355.2, 2004

48. ACI Committee. Code Requirements for nuclear safely related concrete structures. ACI Comm, ACI 349R-9, 1990